ADVANCED MATERIALS
www.advmat.de

Control of Molecular Orbital Ordering Using a van der Waals Monolayer Ferroelectric

*Mohammad Amini, Orlando J. Silveira, Viliam Vaňo, Jose L. Lado, Adam S. Foster, Peter Liljeroth, and Shawulienu Kezilebieke**

2D ferroelectric materials provide a promising platform for the electrical control of quantum states. In particular, due to their 2D nature, they are suitable for influencing the quantum states of deposited molecules via the proximity effect. Here, electrically controllable molecular states in phthalocyanine molecules adsorbed on monolayer ferroelectric material SnTe are reported. The strain and ferroelectric order in SnTe are found to create a transition between two distinct orbital orders in the adsorbed phthalocyanine molecules. By controlling the polarization of the ferroelectric domain using scanning tunneling microscopy (STM), it is successfully demonstrated that orbital order can be manipulated electrically. The results show how ferroelastic coupling in 2D systems allows for control of molecular states, providing a starting point for ferroelectrically switchable molecular orbital ordering and ultimately, electrical control of molecular magnetism.

1. Introduction

The use of electric fields is a powerful approach to manipulate molecular electronic states,[1–7] and consequently, optical properties, adsorption structures, vibrational frequencies, oxidation states and chemical reactivity.[3,8–14] Being able to study these effects at the single molecule level would be very important for understanding the intimate interaction between molecules and their electrostatic environment. Yet, performing such an experiment in a well-controlled manner has proven to be extremely difficult and scanning tunneling microscopy (STM) has emerged as a leading technique in this challenging field.[15–17] In STM, a significant electric field is present between the STM tip and the sample surface, which will induce a Stark shift of the electronic states observed in the tunneling spectra.[18,19] By increasing the set-point tunneling current, the tip–sample distance decreases, leading to increasing electric field strength. Although this is a powerful experimental technique to study the effect of external electric fields on molecular electronic states, molecules are often required to be decoupled from a metallic substrate,[20–22] due to the strong perturbation of their electronic states by hybridization, charge transfer, and screening with the metal substrate.[23,24] Finally, the tunneling current and electric field are linked and using high tunneling currents often leads to instabilities in the tip–molecule-sample junction.

We overcome these limitations by coupling single molecules with two-dimensional ferroelectric (2D-FE) materials as shown schematically in **Figure 1**a. By controlling the charge polarization $\vec{P}$ of the FE, one can tune the electric field experienced by the molecules and consequently, their electronic states. This setup has the distinct advantage that the polarization direction of the FE substrate can be independently controlled and switched irrespective of the electric field from the STM tip. In addition, due to the semiconducting nature of the ferroelectric substrate, it effectively decouples the molecule from the metallic substrate, which gives access to the electronic states of essentially an isolated molecule. Here, we use a monolayer of tin telluride (SnTe) as our FE substrate (see Experimental Section). It has two polarization states ($P\uparrow$ and $P\downarrow$) that are stable up to room temperature and that can be switched by an external electric field.[25]

As a prototype system, we focus on iron-phthalocyanine (FePc) molecules adsorbed on a 2D-FE SnTe substrate (Figure 1a). FePc molecules have partially empty d orbitals in the central metal atom that cause interesting magnetic properties.[26,27] We use low-temperature STM and scanning tunnelling spectroscopy (STS) to study how the molecular states are affected by an in-plane electric field from the 2D-FE SnTe substrate. In particular, we show that the orbital filling and degeneracy of d orbitals of a single FePc changes due to the presence of electric field from the SnTe substrate. This intriguing

M. Amini, O. J. Silveira, V. Vaňo, J. L. Lado, A. S. Foster, P. Liljeroth
Department of Applied Physics
Aalto University
Aalto FI-00076, Finland
A. S. Foster
WPI Nano Life Science Institute (WPI-NanoLSI)
Kanazawa University
Kakuma-machi, Kanazawa 920-1192, Japan
S. Kezilebieke
Department of Physics
Department of Chemistry and Nanoscience Center
University of Jyväskylä
Jyväskylä FI-40014, Finland
E-mail: kezilebieke.a.shawulienu@jyu.fi
The ORCID identification number(s) for the author(s) of this article can be found under https://doi.org/10.1002/adma.202206456.

DOI: 10.1002/adma.202206456

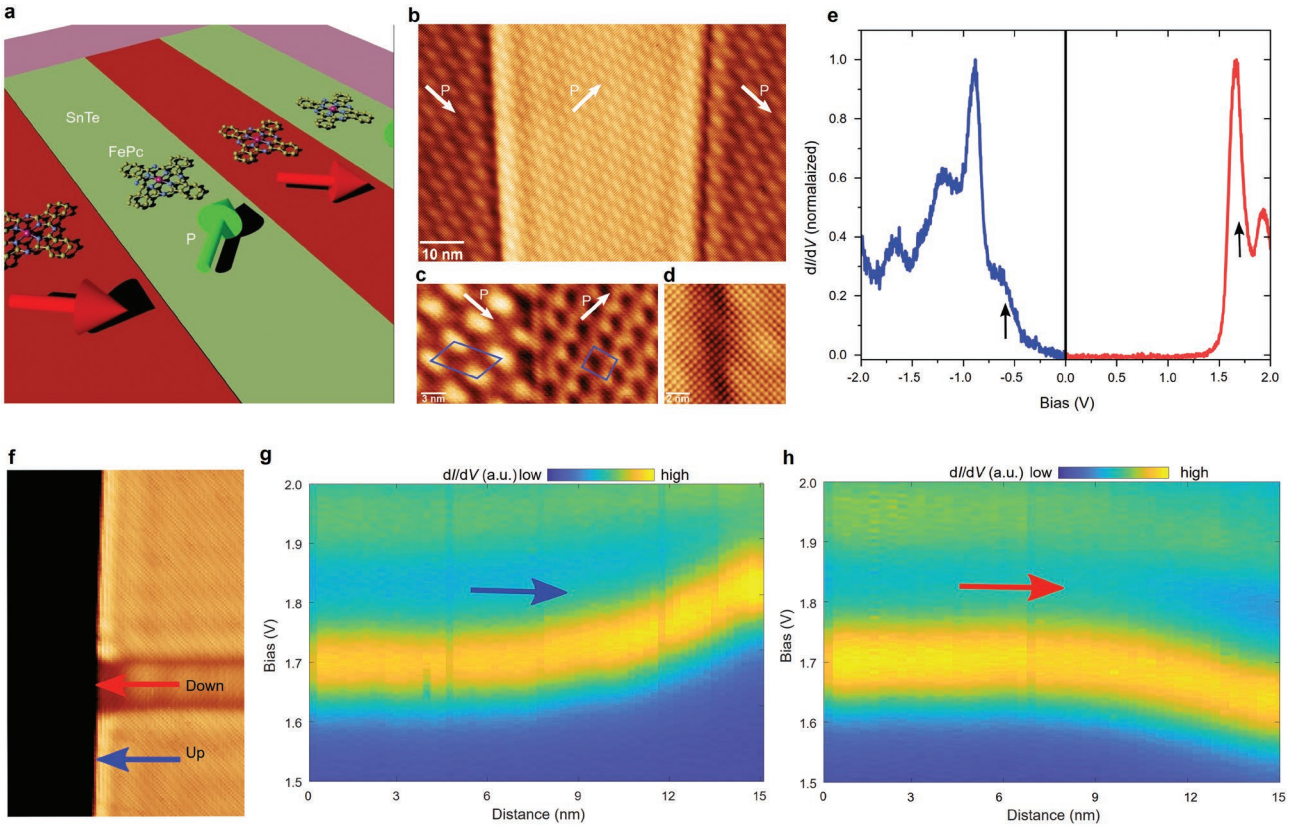

Figure 1. a) Schematics of the FePc molecules on SnTe (green and red area show the ferroelectric domains and the arrows show the direction of electric polarization in each domain). b–d) STM images of the domain formation, moiré pattern, and atomic resolution of the SnTe monolayer, respectively (the white arrows show the direction of the electric polarization. Set points for (b–d), respectively: $I = 2$ nA, $V = 0.5$ V, $I = 100$ pA, $V = 1.5$ V, $I = 100$ pA, $V = 0.1$ V). e) Differential conductance (dI/dV) spectrum on SnTe (set point: $I = 1$ nA, $V = -2$ V for blue spectrum and, $I = 1$ nA, $V = 2$ V for red spectrum). f) STM scan on SnTe shows bright and dark edges corresponding to band bending up (g) and down (h), respectively. g–h) Line spectra taken over 15 nm distance to the edge of the island as shown with blue and red arrows in (f).

phenomenon stems from distinct metal d-orbital occupation caused by electron transfer and energy-level shift associated with the polarization switch of the SnTe monolayer (Figure 1a). Furthermore, it is possible to manipulate the molecular states by controlling the polarization of the FE domain using STM. Finally, we have compared our experimental results with density-functional theory (DFT) calculations, which further support the effects caused by in-plane electric fields on the FePc molecular states. Our study provides a well-defined, controllable platform for manipulation of molecular electronic states with an electric field, having also great potential for practical applications in molecular electronic and spintronic devices.

2. Results and Discussion

We first study the FE order of ultrathin SnTe monolayer grown by molecular beam epitaxy (MBE) on highly oriented pyrolytic graphite (HOPG) substrate (see Experimental Section and Figure S1, Supporting Information). Figure 1b shows an atomically resolved STM image of the SnTe monolayer with stripe domains, which are consistent with the domain structures observed on SnTe monolayer grown on a graphene substrate.[25] The STM topography also exhibits a clear, well-ordered superstructure arising from the moiré pattern between the quasi-square SnTe lattice and hexagonal HOPG lattice. A detailed analysis of moiré pattern between SnTe lattice and hexagonal HOPG lattice can be found in the Supporting Information (see Figures S4 and S5, Supporting Information). As shown in Figure 1c, the domains with different polarization directions have different moiré unit cells due to the different distortion of the SnTe lattice. Finally, it is important to note that the lattice is continuous across the domain boundary as shown in Figure 1d. Figure 1e shows the typical differential conductance (dI/dV) spectra acquired on monolayer SnTe (in the middle of the domain). The dI/dV signal of conduction and valence bands has a large difference in intensity and we use different tunneling conditions for positive and negative bias (red and blue lines, respectively). The arrows in the dI/dV curve (Figure 1e) indicate the band edges giving a bandgap of 1.85 eV. The corresponding dI/dV maps of domains with different polarization can be found in Figure S11 (Supporting Information).

As was shown previously,[25,28,29] ferroelectric materials possess four characteristic features: the formation of the domain structure, the presence of a lattice distortion and band-bending, and the possibility to manipulate the domain structure by external electric fields. As shown in Figure 1b and Figure S1a (Supporting Information), we have observed clear domain structure in our

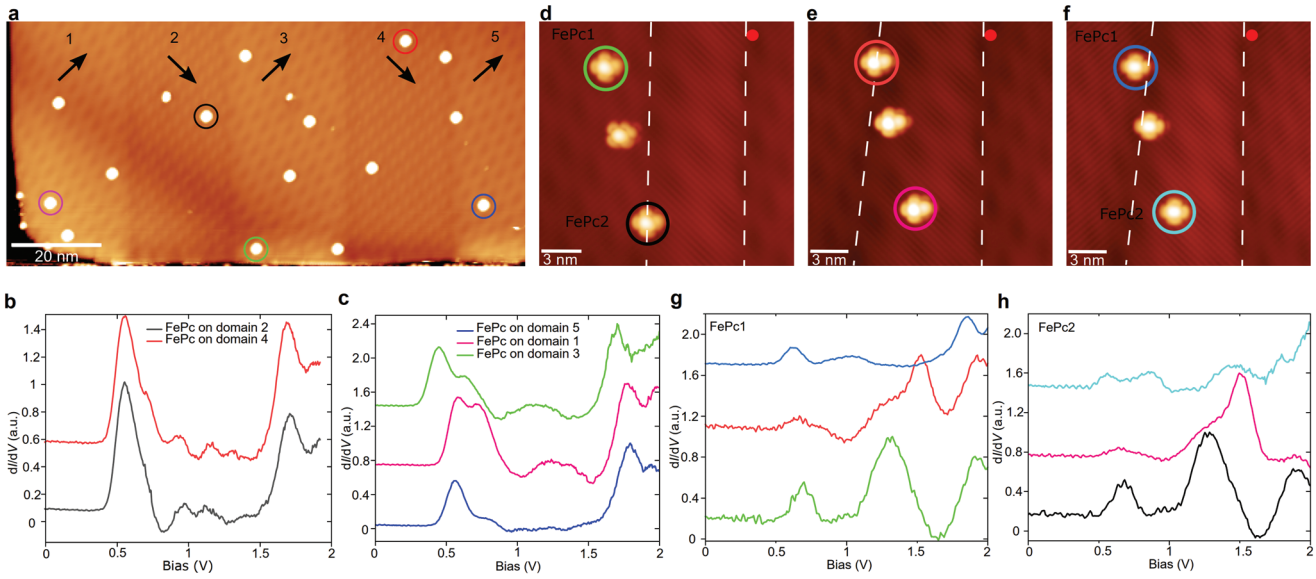

Figure 2. a) Atomically resolved STM image of the SnTe monolayer with FePc molecules (image size 120 × 55 nm^2, $V = 2$ V, $I = 0.3$ nA). b) dI/dV spectra taken on FePcs sitting on domain 2 (indicated with black circle) and domain 4 (indicated with red circle). c) dI/dV spectra taken on FePcs sitting on domain 1 (indicated by the pink circle), domain 3 (indicated by the green circle) and domain 5 (indicated by the blue circle). d–f) Manipulation of the ferroelectric domains using 4V bias voltage pulses applied at the position marked with the red dot. g,h) Point spectra taken on FePc 1 and 2 in (d) and (f) while manipulating the domains.

STM topography. Moreover, a detailed analysis of atomically resolved images further reveals that the lattice is slightly distorted from a perfect square to a parallelogram (see Figure S1b, Supporting Information). The signatures of band-bending can be observed by following the conduction band edges at 1.7 V in the dI/dV curves as a function of the distance to a SnTe island edge seen in Figure 1f. Spatially resolved dI/dV spectra (Figure 1g,h) are taken along the lines perpendicular to the edges of two adjacent domains (blue and red arrows in Figure 1f). The conduction band onsets shift to opposite directions by up to 0.12 eV with a screening length of ≈10 nm. Based on the band bending and the direction of lattice distortion, we can unambiguously determine the in-plane polarization direction (see Figure S1b, Supporting Information). Finally, we use a voltage pulse (4V) between the STM tip and the sample to successfully manipulate the FE polarization through domain wall motion (see Figure S2, Supporting Information). The above observations uniquely demonstrate the existence of ferroelectricity in the system.

Having demonstrated the ferroelectricity of monolayer SnTe by structural and spectroscopic measurements, we now turn to the coupling of this electronic order with magnetic molecular states in a single molecule. **Figure 2**a shows topographic STM images of isolated FePc molecules that are adsorbed on different FE domains on SnTe. The direction of the polarization is indicated by arrows in Figure 2a; these directions can be determined by lattice distortion together with the sign change of polarization charge on edges. Inspection of atomically resolved images demonstrates that FePc has two adsorption geometries which are rotated 45° with respect to each other, with the central Fe atom either sitting on top of an Sn atom or on top of a Te atom of the underlying SnTe surface (see Figure S6, Supporting Information). DFT calculations confirm these two configurations as the most stable ones, and that both the adsorption site and the angle between the FePc molecule and the SnTe substrate play an important role for the stability of the system. The most energetically stable case is when the central atom Fe of the FePc molecule sits on top of Sn while one of the arms of the molecule (the line formed by two consecutive benzene rings) has an angle of $\theta = 45°$ with one of the SnTe lattice vectors. The second most stable configuration (135 meV higher total energy) occurs when the central atom sits on top of Te while $\theta = 0°$ (see Figure S6, Supporting Information). In both cases the FePc molecule keeps its planar geometry, and the Fe–Sn and Fe–Te distances are, respectively, 3.62 and 3.31 Å. Additionally, the SnTe lattice parameters and its intrinsic polarization are not strongly affected by the presence of the molecule. The smaller lattice parameter of the 5 × 5 SnTe supercell in both cases is 2.28 nm, while the largest parameter is 2.5% larger.

Figure 2b,c show dI/dV point spectra taken on different molecules (spectra were obtained by positioning the tip over the central Fe atom and the molecule positions are marked with circles in Figure 2a) with the same adsorption site (the central iron atoms sits on top of Te atoms) and same orientation but located on different domains. The corresponding dI/dV spectra on FePc molecules with different adsorption sites can be found in Figure S13 (Supporting Information). As the direction of the ferroelectric polarization varies from domain to domain between two different values, molecules on domains 1, 3, and 5, and molecules on domains 2 and 4 feel the same polarization direction, respectively. The spectrum obtained on the molecules show three main peaks at ≈0.6, 1.2 and 1.8 V. The peaks at ≈ 0.6 V and 1.2 V can be interpreted as resonances originating from the lowest unoccupied molecular orbital LUMO and the LUMO+1. The peak located at ≈ 1.8 V corresponds to the SnTe conduction band, which also shifts slightly depending on the exact location where the spectra were measured (the

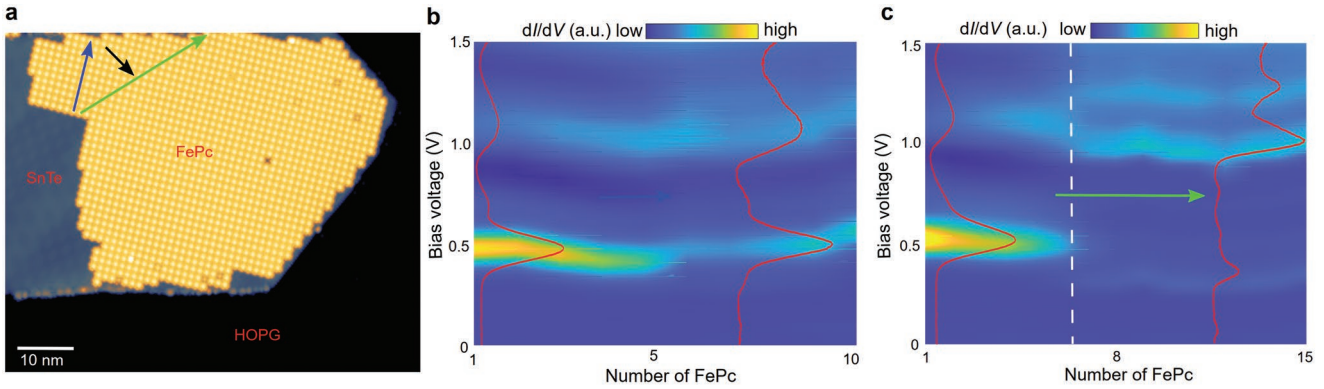

Figure 3. a) FePc island on SnTe (image size 80×60 nm^2, $V = 1.5$ V, $I = 300$ pA). b) Line spectra over a distance of 12.5 nm inside a single FE domain (blue arrow). c) Line spectra over 27 nm crossing two domains (green arrow. Black arrow shows the position of boundary between two domains). The spectra shown as red lines in (b) and (c) correspond to the first and last spectrum in the color scale plot.

corresponding dI/dV maps of molecular orbitals can be found in Figure S10, Supporting Information). Interestingly, the energy position and intensity of the LUMO and LUMO+1 resonances change depending on the polarization of FE domain. In particular, the single LUMO peak of FePc adsorbed on domain 2, 4 (Figure 2b) splits when they are adsorbed on domain 1, 3, 5 (Figure 2c). Furthermore, there are less intense features at around 1 V, which may come from further splitting of LUMO+1 peaks. We will discuss this in more detail in **Figure 3**.

In order to follow the relation between polarization of an FE domain and a change in the molecular states, we have performed a controlled ferroelectric domain manipulation by applying bias voltage pulses with an STM tip. The domain manipulation process is demonstrated as a series of pulses applied with the STM tip placed at the red dot shown in Figure 2d–f. During the domain manipulation, the position of the top and bottom molecules is not changed, only the FE domain under the molecule is manipulated in a controlled manner. The corresponding dI/dV point spectra taken after each manipulation step are shown in Figure 2g,h. Again, the change in the molecular states corresponds to the change of the domain manipulation. In particular, the energy position and intensity of the molecular resonances changes depend on the polarization of FE domain.

It is important to note that the voltage pulses also affect the final condition of the tip and hence the STS. In order to reliably show the effect of electric field caused by the ferroelectric layer on the molecular states, we have created an array of molecules. This allows us to investigate the molecular states as a function of position both within the same domain and across domains without an undesired changes of the STM tip apex. Figure 3a shows densely-packed islands of FePc molecules on top of SnTe (see Experimental Section). This results in FePc islands that span multiple ferroelectric domains of the SnTe layer. We probed the effect of the ferroelectric domains on the dI/dV spectra by first measuring the molecular spectra over a single ferroelectric domain (blue arrow in Figure 3a). As we can see in Figure 3b, the spectra show some variations, but are qualitatively similar. There are two set of peaks at ≈0.5 V and 1.2 V, which correspond to the LUMO and LUMO+1, respectively. The peak positions shift along the band bending of the SnTe layer. The effect of electric field on the molecules in the edge of the domain is stronger than on the molecules in the middle, as can be clearly seen from the last part of line spectra in Figure 3b.

We can also visualize the changes from one ferroelectric domain to another across the boundary between the domains. This is shown in the line spectra on the molecules along the green arrow. We observe that in crossing the boundary between two domains (black arrow in the Figure 3a), there is a discrete change in the dI/dV spectra (the FE domain boundary is indicated by the white dashed line in Figure 3c). In particular, we observe that the original LUMO and LUMO+1 peaks split and intensities are inverted once the direction of polarization changes. This is consistent with our observations on single molecules discussed above. It is important to note that this splitting is not related to where the molecules are located with respect to the underlying moiré pattern. In fact, the moiré pattern only periodically modulates the energy position of the conduction band of SnTe (see Figure S4, Supporting Information). We have repeated the same experiment on different FePc islands and always observe the same behavior (see Figure S7, Supporting Information). The main reason for this change is the Stark effect, which shifts and splits of molecular resonances due to the presence of an external electric field.[30] However, in our case, the electric field comes from the underlying FE substrate and it is not related to the electric field from the STM tip.[16,17] Under this electric field, the D_{4h} symmetry of FePc molecule is broken due to the coupling with ferroelectricity, and this further causes splitting of the partially occupied d_{xz} and d_{yz} levels of the FePc molecules as predicted by our DFT calculations (see details below).

We have performed DFT calculations in order to understand the ground state and electronic properties of the FePc molecules in the presence of ferroelectricity from the SnTe substrate. The ground state of the isolated FePc molecule is a triplet $S = 1$ state, with the spin polarization mostly concentrated on the central Fe atom, as has been predicted before through DFT and Monte Carlo simulations.[26,27,31] We confirmed the magnetic ground state of FePc on SnTe experimentally by following the inelastic spin-flip excitations that can be measured by scanning tunneling spectroscopy in Figure S12 (Supporting Information). The Fe 3*d*-electrons can also manifest the triplet state in different ways

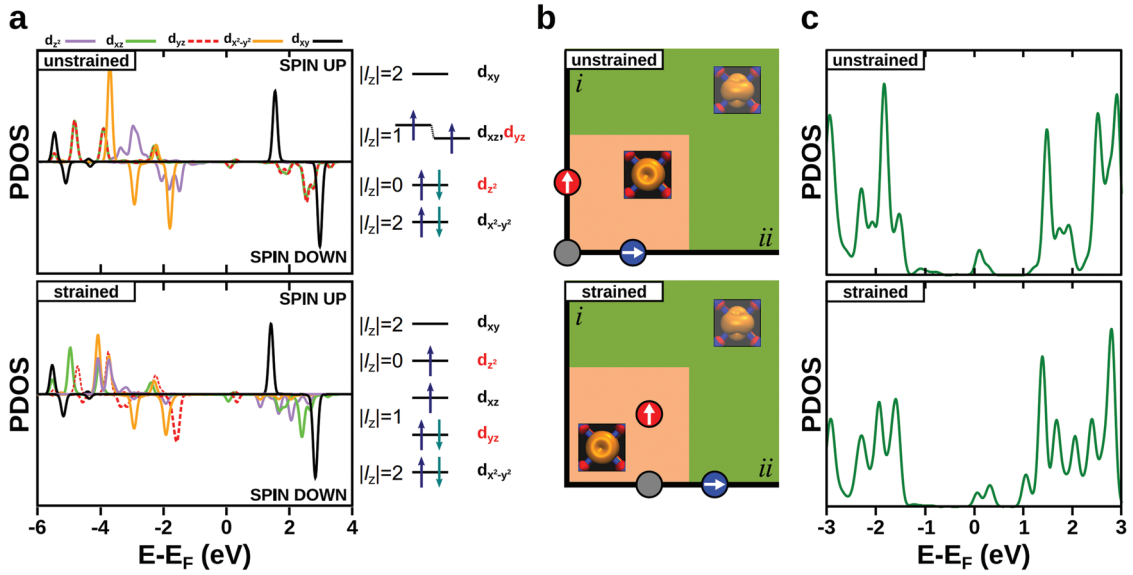

Figure 4. a) Projected density of states on the d orbitals of the Fe atom in the FePc molecule. The energy levels show the orbital transition caused by coupling with ferroelectricity. b) Schematic phase diagram of the FePc orbital state as a function of the strain in the system. The salmon pink and green regions represent the different states of the FePc molecule with the insets showing the spin density around Fe in the two states (isosurface 0.005 a.u.). The *i* and *ii* axes represent the amount of strain in the system. The circles indicate the state of the FePc molecule in the case of no ferroelectric polarization (gray), vertical polarization (red) and horizontal polarization (blue). The top panel shows the FePc state in the different ferroelectric domains without additional strain. A rotation of 90° of the ferroelectric polarization will not affect FePc overall electronic configuration. On the other hand, the bottom panel indicates the FePc state in different ferroelectric domains with additional strain in the layer. Two configurations with ferroelectric polarization rotated by 90° (red and blue circles) give rise to a change in the electronic configuration of the FePc molecule. c) Total density of states of the Fe atom in the FePc+SnTe system.

depending on the interaction with the substrate, and even a high spin quintuplet can be observed when FePc islands are deposited on a Cu surface.[32,33] Here, we demonstrate that the triplet can also correspond to different spin configurations depending on the coupling of the FePc molecule with the ferroelectricity of the SnTe substrate. From the atomic resolution of the SnTe in HOPG in Figure S1 (Supporting Information), different ferroelectric domains are observed with different lattice parameters, where the ferroelectric polarization points towards the direction of the larger lattice parameter. In our calculations, the different domains were simulated by artificially applying a positive strain to the already larger lattice parameter of the SnTe layer, thus increasing its ferroelectric polarization. Fully relaxing the FePc+SnTe system gives a lattice distortion of 2.5%, which is the unstrained case, and the strained case is considered by increasing the distortion to 4%, which matches the largest distortion observed in the experiment (see Figure S1, Supporting Information). **Figure 4**a shows that the D_{4h} tetragonal symmetry is slightly broken due to the coupling with ferroelectricity, and a subtle splitting of the partially occupied d_{xz} and d_{yz} levels is observed. Applying strain to the SnTe layer, hence increasing the coupling of the Fe states with the ferroelectricity, causes the promotion of one electron from the d_{z^2} to the d_{yz} orbital. This transition driven by the combination of ferroelectricity and strain can be rationalized in terms of the low energy crystal field Hamiltonian of the molecule. In particular, given the symmetry of the system, the single-particle crystal field Hamiltonian for the Fe d-orbitals takes the form

$$H = \alpha_0 l_z^2 + \alpha_1 (l_x^4 + l_y^4) + \alpha_2 l_z^4 + \alpha_3 (l_x^2 - l_y^2) \quad (1)$$

where l_x, l_y, l_z are the single-particle angular momentum operators in the Fe d-manifold. The physical significance of the different terms can be understood as follows. The terms α_0 and α_2 account for the planar nature of the molecule, α_1 for the fourfold rotational symmetry and α_3 controls the induced breaking of rotational symmetry induced by the ferroelectric strained substrate. We first note that in the absence of strain in the sample, the two directions of the ferroelectric polarization would be equivalent due to the original C_4 symmetry of the substrate. In this scenario, ferroelectric polarizations rotated by 90° must give rise to equivalent spectra due to symmetry, as depicted schematically in Figure 4b. In contrast, in the presence of strain in the sample, two configurations with ferroelectric polarization rotated by 90° will give rise to inequivalent electronic configurations, due to the explicit breaking of C_4 created by the strain. In this scenario, the two ferroelectric configurations will induce different values of $|\alpha_3|$ in the molecule, effectively allowing to control its state by the polarization of the underlying substrate. For small values of $|\alpha_3|$, the crystal field gives rise to a spin density located in the d_{xz} and d_{yz} orbitals. Once the induced breaking driven by the strain ferroelectric surpasses a critical value, the term α_3 drives an orbital ordering transition yielding a spin polarization located in the d_{z^2} and d_{xz} orbitals. The schematic image in Figure 4b shows the spin densities obtained through DFT around the Fe atom before and after the FePc undergoes the orbital transition. In particular, the symmetry breaking induced by $|\alpha_3|$ drives a splitting between the originally degenerate d_{xz} and d_{yz} manifold, accounting for the orbital transition in the molecule. Figure 4c shows that the orbital transition changes

considerably the density of states of the Fe atom, mostly because the d_{z^2} orbital is partially occupied after the transition, explaining the different dI/dV spectra obtained when the FePc molecule is deposited in different domains. Figure S8 (Supporting Information) shows that the density of states projected on all atoms of the FePc molecule is strongly affected by the coupling with ferroelectricity as well.

3. Conclusion

We have proposed a new platform for probing the effect of an electric field on molecular orbitals by coupling single molecules with a 2D ferroelectric material, with the possibility to manipulate the molecular states by controlling the polarization of the FE domains. In particular, we have demonstrated that under the presence of an intrinsic electric field from the underlying FE substrate, the orbital filling and degeneracy of d orbitals of a single FePc changes. The change in the orbital filling corroborates with a simple model which considers the ferroelectricity associated to the strain on the FE substrate. This provides a promising way to achieve nonvolatile switching of magnetism at the molecular scale by a 2D ferroelectric substrate and has great potential for practical applications in logic and spintronics devices. As we control the magnetism in a single molecule through the FE polarization, it is also a first step towards constructing artifical multiferroic states in molecule–2D material hybrids.

4. Experimental Section

Molecular-Beam Epitaxy (MBE) Sample Growth: An SnTe monolayer was grown by molecular beam epitaxy (MBE) on highly oriented pyrolytic graphite (HOPG) under ultrahigh vacuum conditions (UHV, base pressure $\approx 1 \times 10^{-10}$ mbar). HOPG crystal was cleaved and subsequently out-gassed at ≈300 °C. We deposited SnTe (purity: 99.999% trace metals basis from Sigma–Aldrich) by sublimation from a powder onto the substrate held at ≈210 °C. The deposition temperature of the SnTe was ≈550 °C and deposition time was 1 h. Single, isolated FePc molecules were deposited onto the sample inside the STM at $T = 4$ K. FePc monolayer islands were grown by first depositing the FePc molecules onto the substrate at 4 K and then annealing the sample at 200 °C for 10 min.

Sample Characterization: All the measurements were performed at $T = 4$ K except IETS measurement at 350 mK. STM images were taken in the constant current mode. dI/dV spectra were recorded by standard lock-in detection while sweeping the sample bias in an open feedback loop configuration, with a peak-to-peak bias modulation of 5 mV (long-range spectra) or 0.2 mV (short-range spectra) at a frequency of 709 Hz.

DFT Calculations: DFT+U calculations were performed using the Cococcioni and de Gironcoli simplified version[34] in the QUANTUM ESPRESSO package,[35] where the Hubbard U parameter for the Fe 3*d* orbitals was chosen to be 4 eV. Electron–ion interactions were represented by ultrasoft pseudopotentials generated with the Rappe–Rabe–Kaxiras–Joannopoulos recipe.[36] The electronic exchange-correlation potential was calculated using the Perdew–Burke–Ernzerhof (PBE) functional,[37] and vdW corrections were taken into account through the empirical DFT-D3 Grimme scheme.[38] Electronic wave functions were expanded in plane waves with an energy cutoff of 46 Ry, while the cutoff for the charge density was 326 Ry. The atomic positions of both the gas phase FePc molecule and FePc + SnTe were optimized until the residual forces were <0.001 Ry a.u.$^{-1}$ Spin polarization was considered in all calculations where the FePc molecule was present, with a starting magnetization of 2 μ_B per Fe atom. Different spin configurations were obtained by manipulating the occupation matrix U within the DFT+U method.

Supporting Information

Supporting Information is available from the Wiley Online Library or from the author.

Acknowledgements

This research made use of the Aalto Nanomicroscopy Center (Aalto NMC) facilities and was supported by the European Research Council (ERC-2021-StG no. 101039500 "Tailoring Quantum Matter on the Flatland" and ERC-2017-AdG no. 788185 "Artificial Designer Materials") and Academy of Finland (Academy professor funding nos. 318995 and 320555, Academy research fellow nos. 331342, 336243 and no. 338478 and 346654). A.S.F. was supported by the World Premier International Research Center Initiative (WPI), MEXT, Japan. The authors acknowledge the computational resources provided by the Aalto Science-IT project and CSC, Helsinki.

Conflict of Interest

The authors declare no conflict of interest.

Data Availability Statement

The data that support the findings of this study are available from the corresponding author upon reasonable request.

Keywords

2D van der Waals monolayers, ferroelectric materials, molecular magnetism

Received: July 15, 2022
Revised: December 8, 2022
Published online: January 5, 2023

[1] Y. Li, P. Doak, L. Kronik, J. B. Neaton, D. Natelson, *Proc. Nat. Acad. Sci. USA* **2014**, *111*, 1282.
[2] W. Y. Kim, K. S. Kim, *Acc. Chem. Res.* **2010**, *43*, 111.
[3] P. G. Piva, G. A. Dilabio, J. L. Pitters, J. Zikovsky, M. Rezeq, S. Dogel, W. A. Hofer, R. A. Wolkow, *Nature* **2005**, *435*, 658.
[4] J. Liu, V. V. Laguta, K. Inzani, W. Huang, S. Das, R. Chatterjee, E. Sheridan, S. M. Griffin, A. Ardavan, R. Ramesh, *Sci. Adv.* **2021**, *7*, eabf8103.
[5] S. Wan, Y. Li, W. Li, X. Mao, C. Wang, C. Chen, J. Dong, A. Nie, J. Xiang, Z. Liu, W. Zhu, H. Zeng, *Adv. Funct. Mater.* **2019**, *29*, 1808606.
[6] S. Sahoo, T. Kontos, J. Furer, C. Hoffmann, M. Gräber, A. Cottet, C. Schönenberger, *Nat. Phys.* **2005**, *1*, 99.
[7] M. Pioro-Ladrière, T. Obata, Y. Tokura, Y.-S. Shin, T. Kubo, K. Yoshida, T. Taniyama, S. Tarucha, *Nat. Phys.* **2008**, *4*, 776.
[8] S. Shaik, R. Ramanan, D. Danovich, D. Mandal, *Chem. Soc. Rev.* **2018**, *47*, 5125.

[9] C. F. Gorin, E. S. Beh, M. W. Kanan, *J. Am. Chem. Soc.* **2012**, *134*, 186.
[10] Y. Park, S. Shin, H. Kang, *Acc. Chem. Res.* **2021**, *54*, 323.
[11] M. Alemani, M. V. Peters, S. Hecht, K.-H. Rieder, F. Moresco, L. Grill, *J. Am. Chem. Soc.* **2006**, *128*, 14446.
[12] R. Croce, H. van Amerongen, *Nat. Chem. Biol.* **2014**, *10*, 492.
[13] F. Kulzer, R. Matzke, C. Bräuchle, T. Basché, *J. Phys. Chem. A* **1999**, *103*, 2408.
[14] S. Mangel, M. Skripnik, K. Polyudov, C. Dette, T. Wollandt, P. Punke, D. Li, R. Urcuyo, F. Pauly, S. J. Jung, K. Kern, *Phys. Chem. Chem. Phys.* **2020**, *22*, 6370.
[15] I. Fernández-Torrente, D. Kreikemeyer-Lorenzo, A. Stróżecka, K. J. Franke, J. I. Pascual, *Phys. Rev. Lett.* **2012**, *108*, 036801.
[16] J. Lee, N. Tallarida, X. Chen, L. Jensen, V. A. Apkarian, *Sci. Adv.* **2018**, *4*, eaat5472.
[17] A. Rosławska, T. c. v. Neuman, B. Doppagne, A. G. Borisov, M. Romeo, F. Scheurer, J. Aizpurua, G. Schull, *Phys. Rev. X* **2022**, *12*, 011012.
[18] L. Limot, T. Maroutian, P. Johansson, R. Berndt, *Phys. Rev. Lett.* **2003**, *91*, 196801.
[19] J. Kröger, L. Limot, H. Jensen, R. Berndt, P. Johansson, *Phys. Rev. B* **2004**, *70*, 033401.
[20] J. Repp, G. Meyer, S. M. Stojković, A. Gourdon, C. Joachim, *Phys. Rev. Lett.* **2005**, *94*, 026803.
[21] X. H. Qiu, G. V. Nazin, W. Ho, *Science* **2003**, *299*, 542.
[22] F. Schulz, R. Drost, S. K. Hämäläinen, P. Liljeroth, *ACS Nano* **2013**, *7*, 11121.
[23] F. Tautz, *Prog. Surf. Sci.* **2007**, *82*, 479.
[24] X. Lu, M. Grobis, K. H. Khoo, S. G. Louie, M. F. Crommie, *Phys. Rev. B* **2004**, *70*, 115418.
[25] K. Chang, J. Liu, H. Lin, N. Wang, K. Zhao, A. Zhang, F. Jin, Y. Zhong, X. Hu, W. Duan, Q. Zhang, L. Fu, Q.-K. Xue, X. Chen, S.-H. Ji, *Science* **2016**, *353*, 274.
[26] T. Ichibha, Z. Hou, K. Hongo, R. Maezono, *Sci. Rep.* **2017**, *7*, 2011.
[27] B. de la Torre, M. Švec, P. Hapala, J. Redondo, O. Krejčí, R. Lo, D. Manna, A. Sarmah, D. Nachtigallová, J. Tuček, P. Błoński, M. Otyepka, R. Zbořil, P. Hobza, P. Jelínek, *Nat. Commun.* **2018**, *9*, 2831.
[28] K. Chang, F. Küster, B. J. Miller, J.-R. Ji, J.-L. Zhang, P. Sessi, S. Barraza-Lopez, S. S. P. Parkin, *Nano Lett.* **2020**, *20*, 6590.
[29] Z. Zhang, J. Nie, Z. Zhang, Y. Yuan, Y.-S. Fu, W. Zhang, *Adv. Mater.* **2022**, *34*, 2106951.
[30] R. V. Krems, in *Molecules in Electromagnetic Fields: From Ultracold Physics to Controlled Chemistry*, John Wiley & Sons, New York **2018**, Ch. 2.
[31] A. Mugarza, R. Robles, C. Krull, R. Korytár, N. Lorente, P. Gambardella, *Phys. Rev. B* **2012**, *85*, 155437.
[32] J. Fernández-Rodríguez, B. Toby, M. van Veenendaal, *Phys. Rev. B* **2015**, *91*, 214427.
[33] N. Tsukahara, M. Kawai, N. Takagi, *J. Chem. Phys.* **2016**, *144*, 044701.
[34] M. Cococcioni, S. de Gironcoli, *Phys. Rev. B* **2005**, *71*, 035105.
[35] P. Giannozzi, S. Baroni, N. Bonini, M. Calandra, R. Car, C. Cavazzoni, D. Ceresoli, G. L. Chiarotti, M. Cococcioni, I. Dabo, A. D. Corso, S. de Gironcoli, S. Fabris, G. Fratesi, R. Gebauer, U. Gerstmann, C. Gougoussis, A. Kokalj, M. Lazzeri, L. Martin-Samos, N. Marzari, F. Mauri, R. Mazzarello, S. Paolini, A. Pasquarello, L. Paulatto, C. Sbraccia, S. Scandolo, G. Sclauzero, A. P. Seitsonen, et al., *J. Phys.: Condens. Matter* **2009**, *21*, 395502.
[36] A. M. Rappe, K. M. Rabe, E. Kaxiras, J. D. Joannopoulos, *Phys. Rev. B* **1990**, *41*, 1227.
[37] J. P. Perdew, K. Burke, M. Ernzerhof, *Phys. Rev. Lett.* **1996**, *77*, 3865.
[38] S. Grimme, J. Antony, S. Ehrlich, H. Krieg, *J. Chem. Phys.* **2010**, *132*, 154104.